AIP | Applied Physics Letters

Efficient organic solar cells using copper(I) iodide (CuI) hole transport layers

Ying Peng, Nir Yaacobi-Gross, Ajay K. Perumal, Hendrik A. Faber, George Vourlias, Panos A. Patsalas, Donal D. C. Bradley, Zhiqun He, and Thomas D. Anthopoulos

Citation: Applied Physics Letters **106**, 243302 (2015); doi: 10.1063/1.4922758
View online: http://dx.doi.org/10.1063/1.4922758
View Table of Contents: http://scitation.aip.org/content/aip/journal/apl/106/24?ver=pdfcov
Published by the AIP Publishing

Efficient organic solar cells using copper(I) iodide (CuI) hole transport layers

Ying Peng,[1,2] Nir Yaacobi-Gross,[2] Ajay K. Perumal,[2] Hendrik A. Faber,[2] George Vourlias,[3] Panos A. Patsalas,[3] Donal D. C. Bradley,[2] Zhiqun He,[1,a)] and Thomas D. Anthopoulos[2,a)]
[1]*Key Laboratory of Luminescence and Optical Information, Ministry of Education, Institute of Optoelectronic Technology, Beijing Jiaotong University, Beijing 100044, People's Republic of China*
[2]*Department of Physics and Centre for Plastic Electronics, Blackett Laboratory, Imperial College London, London SW7 2AZ, United Kingdom*
[3]*Department of Physics, Laboratory of Applied Physics, Aristotle University of Thessaloniki, GR-54124 Thessaloniki, Greece*

(Received 12 April 2015; accepted 6 June 2015; published online 16 June 2015)

We report the fabrication of high power conversion efficiency (PCE) polymer/fullerene bulk heterojunction (BHJ) photovoltaic cells using solution-processed Copper (I) Iodide (CuI) as hole transport layer (HTL). Our devices exhibit a PCE value of ~5.5% which is equivalent to that obtained for control devices based on the commonly used conductive polymer poly(3,4-ethylenedioxythiophene): polystyrenesulfonate as HTL. Inverted cells with PCE >3% were also demonstrated using solution-processed metal oxide electron transport layers, with a CuI HTL evaporated on top of the BHJ. The high optical transparency and suitable energetics of CuI make it attractive for application in a range of inexpensive large-area optoelectronic devices. © *2015 AIP Publishing LLC*.
[http://dx.doi.org/10.1063/1.4922758]

Organic photodiodes hold tremendous potential for a range of applications encompassing solar and indoor energy harvesting (organic photovoltaics (OPVs)), sensing,[1–3] and imaging.[4,5] This is primarily due to the combination of a processing versatility that could lead to scalable and low-cost manufacturing and their potential for mechanical flexibility.[6] It is now established that the performance of state-of-the-art diodes is highly dependent on the interfaces between the conductive electrodes and organic semiconductors.[7,8] Thin layers are often incorporated to accurately tune the interfacial electronic structure, with ideal interlayer materials also possessing high optical transparency and electrical conductivity and supporting simple low-temperature processing methods. In an effort to identify and/or develop such interlayer technologies, a range of materials systems have recently been considered and implemented in OPV cells.[9,10] Amongst these, the conductive polymer poly(3,4-ethylenedioxythiophene): polystyrenesulfonate (PEDOT:PSS) is the most studied hole transport layer (HTL). It has a work function of ~5 eV and supports Ohmic contact between many donor materials and the commonly used indium tin oxide (ITO) anode. In addition, PEDOT:PSS helps to planarize and stabilize the ITO surface. It is, however, processed from water which is hard to fully exclude from the photoactive layer where it can initiate unwanted chemical reactions.[11] It is also acidic, causing corrosion of the ITO anode[12] and not very effective as an electron blocking material.[13] In an effort to address some/all of these issues, a range of alternative HTL materials have been investigated, including PSS-free vapor phase polymerized PEDOT,[14,15] graphene oxide,[16] carbon nanotubes (CNTs),[17] polyaniline (PANI),[18] p-type metal oxides (e.g., V_2O_5, MoO_3 (Ref. 19), and NiO (Ref. 20)) and most recently CuSCN.[21] Despite significant progress there is still a need for better-optimized HTL materials.

Copper (I) Iodide (CuI) is an ionic solid that has recently been shown to have potential as a HTL for application in organic optoelectronics.[22] It exhibits three crystalline phases, namely, α, β, and γ,[23] of which the γ-CuI zinc blende structure (cubic), known to form at deposition temperatures below 390 °C, is the most interesting for our purpose. γ-CuI is a p-type, wide-bandgap (~3.1 eV)[24] semiconductor and, due to its optical transparency and favourable Fermi level energy, has previously been used as a HTL in solid-state dye-sensitized solar cells.[25] CuI has also been incorporated in organic light emitting diodes (OLEDs)[26] and organic solar cells.[22] For example, Shao *et al.*[27] recently reported OPV cells (power conversion efficiency (PCE) ≈ 3.1%) employing thermally evaporated CuI as HTL. CuI has also been used as a p-dopant in hole transporting layers for OPV[28] and hybrid perovskite solar cells.[29] Despite these promising initial results, the full potential of CuI as an inexpensive HTL material for high efficiency OPVs has yet to be demonstrated. Here, we report the use of CuI as a HTL in OPV cells with bulk-heterojunction (BHJ) blends of poly(di(2-ethylhexyloxy) benzo[1,2-b:4,5-b′]dithiophene-co-octylthieno[3,4-c]porrole-4,6-dione) (PBDTTPD)[30] and [6,6]-phenyl-C61-butyric acid methyl ester ($PC_{61}BM$) (Figure 1(a)). We demonstrate PCE > 5.5% for standard (bottom-) and >3% for inverted (top-anode) cells, the latter using a solution-processed In_2O_3/ZnO electron transport layer (ETLs) (Figure 1(b)).

Patterned glass/ITO electrodes (40–60 Ω/sq) were cleaned sequentially in soapy water, acetone, de-ionized water, and isopropyl alcohol ultrasonic baths for 5 min each and subsequently dried with nitrogen gas. The substrates were then exposed to UV-ozone for 10 min. CuI solutions were prepared by dissolving copper(I) iodide (Sigma-Aldrich, 99.9%) in acetonitrile at 20 mg/ml and were

a)Authors to whom correspondence should be addressed. Electronic addresses: zhqhe@bjtu.edu.cn and t.anthopoulos@imperial.ac.uk

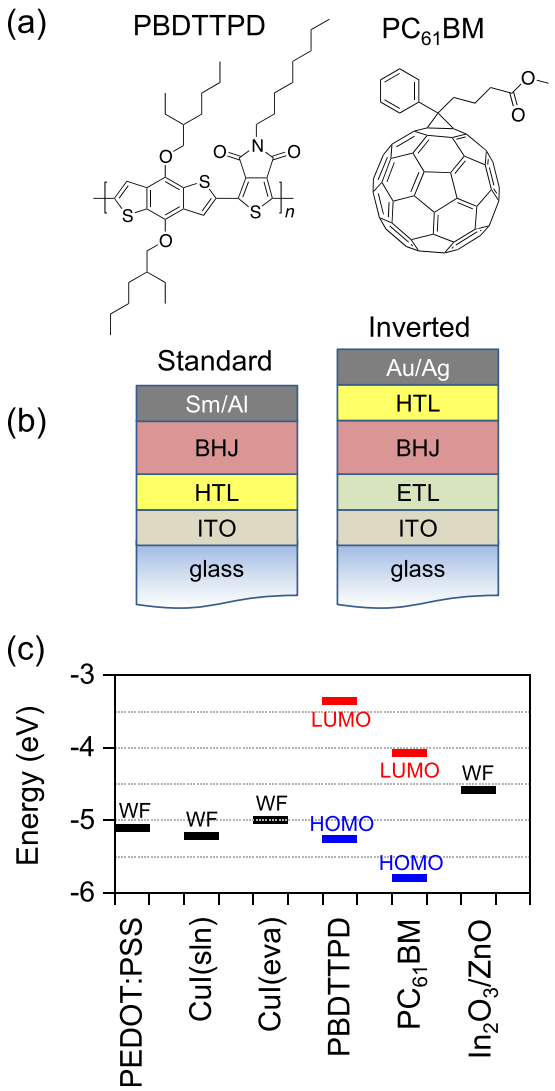

FIG. 1. (a) Chemical structures of the donor polymer (PBDTTPD) and the acceptor fullerene derivative ($PC_{61}BM$) used. (b) Schematic structures of the standard and inverted solar cells. (c) HOMO and LUMO energies for PBDTTPD and $PC_{61}BM$ obtained from Ref. 30, together with the measured work function energies for PEDOT:PSS, CuI(sln), CuI(eva), and In_2O_3/ZnO.

deposited onto the electrodes by spin coating (1500 rpm) in nitrogen followed by an annealing step at 100 °C for 20 min. Reference OPVs were fabricated using PEDOT:PSS (Clevios PVP Al4083) HTL solutions spin-coated at 1000 rpm. Solution mixtures of the donor polymer PBDTTPD and fullerene acceptor $PC_{61}BM$ (1:1.5 wt. % with 15 mg/ml total solid) were spin-coated onto the HTLs at 1000 rpm from chlorobenzene in nitrogen. Bilayer Sm/Al (10/90 nm) cathode electrodes were evaporated in high vacuum (10^{-6} mbar) to complete the cells with active area of 5 mm^2. Inverted solar cells were fabricated using ITO electrodes coated with a bilayer In_2O_3/ZnO ETL. Solutions of In_2O_3 and ZnO were prepared, respectively, by dissolving indium nitrate in 2-methoxyethanol at 30 mg/ml and zinc oxide hydrate in ammonium hydroxide at 10 mg/ml. First, the In_2O_3 precursor was spin-coated at 2500 rpm and subsequently annealed at 200 °C for 30 min in air, which allows Indium nitrate convert to Indium oxide, yielding films of thickness 8–10 nm. ZnO was then spin-coated on top at 2000 rpm and annealed at 200 °C for 30 min in air to produce a 8–10 nm-thick layer. The PBDTTPD:$PC_{61}BM$ blend was next spin-coated, followed by thermal evaporation (10^{-6} mbar) of a 25 nm-thickness CuI HTL. Finally, a bilayer Au/Ag (10/70 nm) anode was thermally evaporated (10^{-6} mbar) on top. Ultraviolet-visible-near infrared (UV-vis-NIR) absorption spectra (200–1400 nm) were measured using a Shimadzu UV-2600 spectrophotometer, while the surface topography of the films using an Agilent 5500 atomic force microscope (AFM). Current density-voltage (J-V) characteristics in nitrogen were obtained with a 2400 Keithley source-meter in the dark and under AM 1.5G simulated solar illumination (100 mW/cm^2). EQE values were calculated from the device spectral response characteristics recorded under mechanically chopped, monochromated light from a 30 W quartz tungsten halogen lamp. During EQE measurements, the active area of each device (5 mm^2) was masked using a stencil mask in order to avoid parasitic current contribution. Work function measurements were performed using a Kelvin probe (KP) system (KP-Technology SK5050), with the absolute work function of the reference and the valence band maximum (VBM) energy of CuI determined using an atmospheric photoemission (AP) system (KP-APS02). During AP measurements, the sample is irradiated with a monochromatic light of varying energy between 6.5 and 3.5 eV and a photocurrent between the sample and a metallic Kelvin probe (tip) placed in close proximity to the sample can be detected. Since only photons with sufficient energy can lead to emission of photoelectrons, the photocurrent increases with increasing photon energy. The ionization energy can then be determined via Fowler analysis.

The highest occupied (HOMO) and lowest unoccupied (LUMO) molecular orbital energies for PBDTTPD and $PC_{61}BM$[30] are shown in Figure 1(c), together with the measured work function (by KP) values for HTLs PEDOT:PSS and CuI and ETL In_2O_3/ZnO. The VBM values for the solution-processed [CuI(sln)] and evaporated [CuI(eva)] CuI layers were determined to be ~5.26 (±0.05) eV and ~5.05 (±0.05) eV, respectively (Figure S1).[31] The Fermi energy (E_F) levels were also measured for these layers by Kelvin probe, yielding ~5.22 and ~5 eV, respectively. The near coincidence of VBM and E_F values points to both CuI layers being heavily p-doped.

X-ray photoelectron spectroscopy (XPS) and X-ray diffraction (XRD) measurements (Figures S2 and S3)[31] were used to probe the differences in chemical composition and crystal structure, respectively, for the CuI(sln) and CuI(eva) layers. XPS measurements reveal that both samples are iodine deficient (Table S1)[31] but that the CuI(sln) films are slightly more so, with [I]/[Cu] = 0.734 *versus* 0.850 for CuI(eva). This difference may explain the slightly different value of the measured work functions between CuI(sln) and CuI(eva). However, further work is needed to clarify this point, possibly using photoluminescence measurements. Furthermore, XRD analysis revealed that both samples exhibit exclusively (111) and (222) peaks, consistent with a dominant γ-CuI zinc blende structure.[24] CuI(eva) films appear, however, to be composed of larger crystallites than CuI(sln) layers (Table S1).[31] Again, this difference may be responsible for the stoichiometric, and hence electronic, differences between the two types of CuI layers.

Figure 2(a) displays the UV-vis-NIR absorption spectra for CuI(sln), CuI(eva), and spin-coated PEDOT:PSS layers. Across the solar-energy-relevant 400–1400 nm range, CuI shows consistently higher transmission than PEDOT:PSS, a desirable property for standard (bottom ITO anode) solar cell use. Both CuI layers exhibit an absorption onset at ~420 nm (2.95 eV), with a sharp peak for CuI(sln) and a shoulder for CuI(eva) at ~404 nm (3.07 eV) that can be assigned to the $Z_{1,2}$ band edge exciton transitions.[24] The higher energy peak at ~336 nm (3.69 eV) is then the associated Z_3 split-off band transition and that at ~258 nm (4.80 eV) the E_1 transition from the top valence band to the conduction band at higher k along the [111] direction.[24] Additional features appear near 371 nm and 381 nm for CuI(eva) and may, in part, arise from the effects of strain[24] but further studies will be needed to confirm or refute this proposal.

The surface topography of the different HTL layers was studied via AFM and Figure 2(b) displays images for 40 nm PEDOT:PSS (2nd from left) and 40 nm CuI(sln) (2nd from right) spin-coated on ITO and for 25 nm CuI(eva) (right) deposited on glass. The surface topography of the ITO substrate (left) is also shown. The extracted root mean square (rms) surface roughness of the latter was ~3.8 nm. PEDOT:PSS tends to planarize ITO electrodes[14] and here exhibited rms values ~1.44 nm. Conversely CuI(sln) more closely conformed to the ITO surface with rms roughness ~4 nm. CuI(eva) on glass is again approximately conformal with rms roughness ~1.17 nm. The difference in the surface roughness is better illustrated in the height histogram of Figure 2(c), where the height distribution of each material surface is plotted on the same axis. It can be seen that smoother surfaces, e.g., glass/ITO/PEDOT:PSS and glass/evaporated CuI, exhibit narrow distributions peaked at smaller height values.

To test the performance of CuI as a HTL in OPV cells, we fabricated standard structures (Figure 1) based on PBDTTPD:PC_{61}BM BHJ blends. PEDOT:PSS HTL standard cells were also fabricated as control devices. Both CuI and PEDOT:PSS HTLs were ~35 nm thickness in order to allow a direct performance comparison. Figure 3(a) displays the current density-voltage (J-V) characteristics measured for one sun illumination (AM1.5G, 100 mW/cm^2), while Figure S4 shows the J-V characteristics measured in the dark.[31] Table I summarizes the various solar cell parameters extracted from the J-V characteristics. It is evident that the CuI(sln) cells exhibit equivalent efficiency (PCE ~ 5.54%) to reference PEDOT:PSS devices (PCE ~ 5.5%). Their high open circuit voltage (V_{OC} = 0.81 V) and reasonable fill factor (FF ~ 0.5) values suggest that these cells do not suffer from either large contact resistances or high bulk resistivities, supporting the potential of CuI as an OPV HTL material. The CuI(sln) cells generate a moderately higher short-circuit current density (J_{SC}) than PEDOT:PSS HTL devices. This is likely to arise from the reduced "parasitic" absorption of CuI compared to PEDOT:PSS (c.f. Figure 2(a)), leading to higher optical absorption within the BHJ blend layer. Finally, we note that as-prepared CuI-based OPVs are chemically stable and continue to work even after storage in the glove box for several months. From these results, we conclude that CuI(sln) can indeed be employed as a HTL in OPV cells in place of PEDOT:PSS.

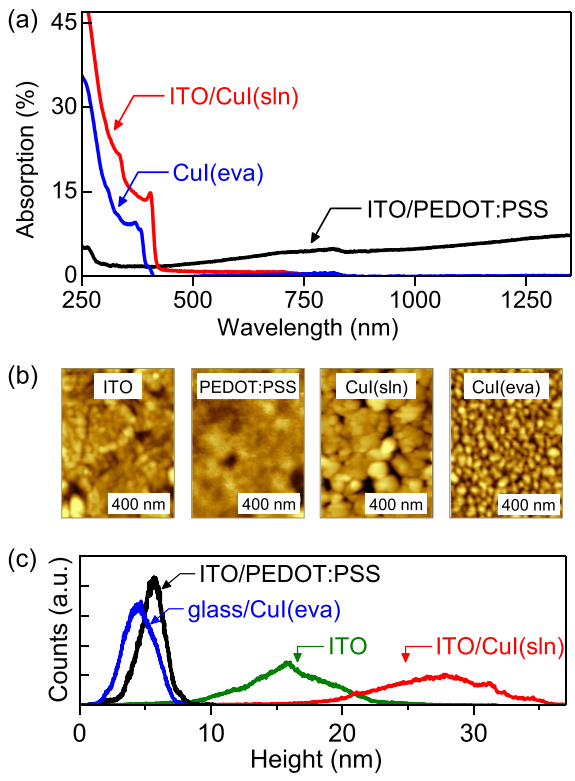

FIG. 2. (a) UV-vis-NIR absorption spectra of PEDOT:PSS and CuI(sln) films on ITO/glass and CuI(eva) on glass. (b) AFM surface topography images of ITO (left), ITO/PEDOT:PSS (2nd left), ITO/CuI(sln) (2nd right), and CuI(eva) (right) on glass. (c) Height histogram extracted from the AFM topography images in (b).

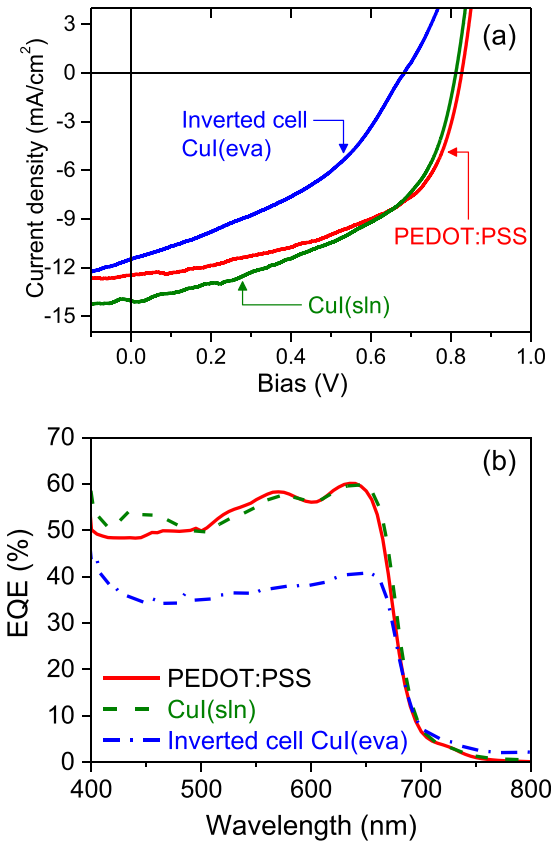

FIG. 3. (a) J-V characteristics and (b) external quantum efficiency (EQE) spectra for standard (with PEDOT:PSS and CuI(sln) as HTL) and inverted (with CuI(eva) HTL) PBDTTPD:PC_{61}BM BHJ blend solar cells.

TABLE I. Operating parameters of standard and inverted OPV cells based on different HTLs.

Device structure	HTL	J_{sc} (mA/cm^2)	V_{oc} (V)	FF	PCE (%)	R_{Sh} (Ω/cm^2)
Standard	PEDOT: PSS	12.4 ($\pm$0.5)[a]	0.83 ($\pm$0.01)[a]	0.54 ($\pm$0.02)[a]	5.50 ($\pm$0.15)[a]	4.9×10^2
	CuI(sln)	14.0 ($\pm$0.2)[a]	0.81 ($\pm$0.01)[a]	0.50 ($\pm$0.01)[a]	5.54 ($\pm$0.08)[a]	3.3×10^2
Inverted	CuI(eva)	11.5 ($\pm$1.6)[a]	0.69 ($\pm$0.04)[a]	0.40 ($\pm$0.02)[a]	3.12 ($\pm$0.38)[a]	1.4×10^2

[a]Standard deviation.

In order to further demonstrate the versatility of CuI as a HTL material, we also fabricated inverted OPV cells (Fig. 1(b)) using In_2O_3/ZnO (40 nm combined thickness) as ETL and CuI(eva) (25 nm) as HTL. Figure 3(a) displays a representative J-V characteristic for such a cell. The device performance is inferior to CuI(sln) HTL standard structure cells, with PCE restricted to 3.12% by significantly reduced V_{OC} and FF values (see Table I). The reduced FF is thought to be due to imperfections/discontinuities in the metal oxide ETL and in particular, the presence of pinholes that lead to leakage currents. A relatively low shunt resistance ($R_{Sh} = 1.4 \times 10^2$ Ω/cm^2) is deduced for the inverted cell relative to the standard CuI(sln) OPV cell ($R_{Sh} = 3.3 \times 10^2$ Ω/cm^2). The reduced V_{OC} value further suggests that the ETL has a negative effect on the cell energetics. These results nevertheless show that CuI and In_2O_3/ZnO have potential, respectively, for HTL and ETL use in inverted OPV cells; further optimization will, however, be required.

We also measured the external quantum efficiency (EQE) spectra for each solar cell (Figure 3(b)), with both standard and inverted devices exhibiting a broad EQE spectra that matches the absorption of the BHJ PBDTTPD: $PC_{61}BM$ blend (not shown). Standard CuI(sln) cells exhibit an EQE that is marginally higher than the reference PEDOT: PSS devices at wavelengths from 400 to ~500 nm, is then marginally lower up to ~600 nm, and finally peaks at a comparable ~60% at 650 nm. In agreement with their lower J_{SC}, our inverted CuI(eva) cells show a lower maximum EQE ~ 40%, again peaking at 650 nm. As already noted above, it is anticipated that it should be possible to increase the PCE of the latter cells by optimization of the ETL.

In summary, we have reported the use of CuI as a HTL material in efficient standard and inverted BHJ OPV cells. CuI(sln) devices based on the standard (ITO bottom anode) architecture show a maximum PCE of ~5.54%, highlighting the potential that CuI has as an inexpensive HTL system. Combination with a low-temperature solution-processed bilayer metal oxide ETL, use of CuI(eva) as HTL and a top Au/Ag anode electrode, also enabled the fabrication of inverted OPV cells with promising performance characteristics.

The authors would like to thank the China Scholarships Council (CSC) for a Ph.D. exchange scholarship, and Y.P. and Z.H. also acknowledge partial support from the NNSF China (Grant No. 21174016). D.D.C.B. is Lee-Lucas Professor of Experimental Physics at Imperial College London.

[1]O. Hofmann, P. Miller, P. Sullivan, T. S. Jones, and D. D. C. Bradley, Sens. Actuators, B **106**(2), 878 (2005).
[2]X. Wang, O. Hofmann, R. Das, E. M. Barrett, and D. D. C. Bradley, Lab Chip **7**(1), 58 (2007).
[3]X. Wang, M. Amatatongchai, D. Nacapricha, O. Hofmann, J. C. de Mello, D. D. C. Bradley, and A. J. de Mello, Sens. Actuators, B **140**(2), 643 (2009).
[4]P. E. Keivanidis, N. C. Greenham, H. Sirringhaus, R. H. Friend, J. C. Blakesley, R. Speller, M. Campoy-Quiles, T. Agostinelli, D. D. C. Bradley, and J. Nelson, Appl. Phys. Lett. **92**(2), 023304 (2008).
[5]T. Agostinelli, M. Campoy-Quiles, J. C. Blakesley, R. Speller, D. D. C. Bradley, and J. Nelson, Appl. Phys. Lett. **93**(20), 203305 (2008).
[6]H. Zhou, Y. Zhang, J. Seifter, S. D. Collins, C. Luo, G. C. Bazan, T.-Q. Nguyen, and A. J. Heeger, Adv. Mater. **25**(11), 1646 (2013).
[7]S. Khodabakhsh, D. Poplavskyy, S. Heutz, J. Nelson, D. D. C. Bradley, H. Murata, and T. S. Jones, Adv. Funct. Mater. **14**(12), 1205 (2004).
[8]N. Tokmoldin, N. Griffiths, D. D. C. Bradley, and S. A. Haque, Adv. Mater. **21**(34), 3475 (2009).
[9]P. Ravirajan, D. D. C. Bradley, J. Nelson, S. A. Haque, J. R. Durrant, H. J. P. Smit, and J. M. Kroon, Appl. Phys. Lett. **86**(14), 143101 (2005).
[10]R. Xia, D.-S. Leem, T. Kirchartz, S. Spencer, C. Murphy, Z. He, H. Wu, S. Su, Y. Cao, J. S. Kim, J. C. deMello, D. D. C. Bradley, and J. Nelson, Adv. Energy Mater. **3**(6), 718 (2013).
[11]K. Kawano, R. Pacios, D. Poplavskyy, J. Nelson, D. D. C. Bradley, and J. R. Durrant, Sol. Energy Mater. Sol. Cells **90**(20), 3520 (2006).
[12]M. P. De Jong, L. J. Van Ijzendoorn, and M. J. A. De Voigt, Appl. Phys. Lett. **77**(14), 2255 (2000).
[13]R. Jin, P. A. Levermore, J. Huang, X. Wang, and D. D. C. Bradley, Phys. Chem. Chem. Phys. **11**(18), 3455 (2009).
[14]P. A. Levermore, L. Chen, X. Wang, R. Das, and D. D. C. Bradley, Adv. Mater. **19**(17), 2379 (2007).
[15]X. Wang, T. Ishwara, W. Gong, M. Campoy-Quiles, J. Nelson, and D. D. C. Bradley, Adv. Funct. Mater. **22**(7), 1454 (2012).
[16]S.-S. Li, K.-H. Tu, C.-C. Lin, C.-W. Chen, and M. Chhowalla, ACS Nano **4**(6), 3169 (2010).
[17]J. Wei, Y. Jia, Q. Shu, Z. Gu, K. Wang, D. Zhuang, G. Zhang, Z. Wang, J. Luo, and A. Cao, Nano Lett. **7**(8), 2317 (2007).
[18]Y.-K. Han, M.-Y. Chang, K.-S. Ho, T.-H. Hsieh, J.-L. Tsai, and P.-C. Huang, Sol. Energy Mater. Sol. Cells **128**, 198 (2014).
[19]V. Shrotriya, G. Li, Y. Yao, C.-W. Chu, and Y. Yang, Appl. Phys. Lett. **88**(7), 073508 (2006).
[20]M. D. Irwin, D. Bruce Buchholz, A. W. Hains, R. P. H. Chang, and T. J. Marks, Proc. Natl. Acad. Sci. **105**(8), 2783 (2008).
[21]N. Yaacobi-Gross, N. D. Treat, P. Pattanasattayavong, H. Faber, A. K. Perumal, N. Stingelin, D. D. C. Bradley, P. N. Stavrinou, M. Heeney, and T. D. Anthopoulos, Adv. Energy Mater. **5**(3), 1401529 (2015).
[22]W. Sun, H. Peng, Y. Li, W. Yan, Z. Liu, Z.-Q. Bian, and C. H. Huang, J. Phys. Chem. C **118**(30), 16806 (2014).
[23]P. M. Sirimanne, M. Rusop, T. Shirata, T. Soga, and T. Jimbo, Mater. Chem. Phys. **80**(2), 461 (2003).
[24]M. Grundmann, F.-L. Schein, M. Lorenz, T. Böntgen, J. Lenzner, and H. von Wenckstern, Phys. Status Solidi A **210**(9), 1671 (2013).
[25]M. Rusop, T. Soga, T. Jimbo, and M. Umeno, Surf. Rev. Lett. **11**(06), 577 (2004).
[26]P. Stakhira, V. Cherpak, D. Volynyuk, F. Ivastchyshyn, Z. Hotra, V. Tataryn, and G. Luka, Thin Solid Films **518**(23), 7016 (2010).
[27]S. Shao, J. Liu, J. Zhang, B. Zhang, Z. Xie, Y. Geng, and L. Wang, ACS Appl. Mater. Interfaces **4**(10), 5704 (2012).
[28]D.-H. Kim, T.-M. Kim, W.-I. Jeong, and J.-J. Kim, Appl. Phys. Lett. **101**(15), 153303 (2012).
[29]J. A. Christians, R. C. M. Fung, and P. V. Kamat, J. Am. Chem. Soc. **136**(2), 758 (2014).
[30]E. T. Hoke, K. Vandewal, J. A. Bartelt, W. R. Mateker, J. D. Douglas, R. Noriega, K. R. Graham, J. M. J. Fréchet, A. Salleo, and M. D. McGehee, Adv. Energy Mater. **3**(2), 220 (2013).
[31]See supplementary material at http://dx.doi.org/10.1063/1.4922758 for further experimental data obtained and relevant analysis.